Mater.Phys.Mech.1 (2000) 1-10

AC MAGNETIC PROPERTIES OF COMPACTED FeCo NANOCOMPOSITES

Anit K. Giri, Krishna M. Chowdary and Sara A. Majetich

Department of Physics, Carnegie Mellon University
Pittsburgh, PA 15213-3890, USA

Received: September 23, 1999

Abstract. Here we report the AC magnetic properties of soft magnetic nanocomposites made from compaction of $Fe_{10}Co_{90}$ nanoparticles. Following a discussion of previous work on soft magnetic nanocomposites, the sample preparation and experimental characterization by AC permeametry are described. The permeability is constant and equal to the DC value for low frequencies, but drops off sharply above a characteristic frequency f_c. A model is developed to explore the relation between f_c and material parameters including the effective anisotropy, exchange coupled volume, temperature, and saturation magnetization.

1. INTRODUCTION

Many recent developments in soft magnets, which are used in power applications, have been based on amorphous and nanocrystalline materials [1-5]. In amorphous solids the magnetocrystalline anisotropy K is by definition equal to zero, eliminating the main material-dependent contribution to the coercivity. The effective anisotropy K_{eff} can also be low in nanocrystalline materials if conditions specified by the Random Anisotropy Model are met [1-3, 6]. The grain size must be smaller than the magnetic exchange length L_{ex}, and the grains must be exchange coupled with their easy axes for magnetization randomly oriented. The combination of random orientation and averaging over multiple grains makes the preference for magnetization in a particular direction, and therefore K_{eff}, very small. Theoretically, low K materials become even softer if the grain size D is small enough. The DC magnetic properties of nanocomposites have been modeled in terms of the Random Anisotropy Model [1-3]. The magnetization reversal field or coercivity H_c is predicted to be proportional to D^6, while the permeability $\mu=B/H$ is predicted to be proportional to D^{-6}. Here we extend this approach to understand the AC magnetic properties of nanocomposites.

Previous work on the AC magnetic properties of bulk magnetic materials has shown that the permeability can be split into in-phase (μ') and out-of-phase (μ") components, just like the permittivity of dielectric materials:

$$\mu = \mu' - i\mu''. \qquad (1)$$

These components obey a Kramers-Krönig relationship [7], so that by knowing the value of one for all frequencies, the other is uniquely determined. The real part μ' is typically flat up to a cutoff frequency, and then drops off, while the imaginary part μ" shows a peak at the same frequency. In the best high frequency ferrite materials, the cutoff frequency is in the GHz range, and is associated with the precession frequency of spins about the applied magnetic field. While high frequency magnetic materials are highly insulating to reduce eddy current losses, their properties have not been analyzed in terms of their microstructure.

A benchmark for soft magnetic materials is the total power loss, P_{tot}, as the material is magnetized and demagnetized. It depends on the hysteresis loss, losses due to the eddy currents created by the changing magnetic field, and anomalous losses associated with domain wall motion [8]. These contributions have different frequency dependencies:

$$P_{tot} = P_{hys} + P_{eddy\ current} + P_{anom} = W_{hys} f + A f^2/\rho + P_{anom}(f). \qquad (2)$$

P_{hys} varies linearly with the frequency f and the area within the hysteresis curve W_{hys}, $P_{eddy\ current}$ is quadratic

Corresponding author: Sara A. Majetich, e-mail: sm70+@andrew.cmu.edu

© 2000 Advanced Study Center Co. Ltd.

in frequency and inversely proportional to the resistivity ρ. A is a constant. The anomalous loss P_{anom} has no fixed power law dependence on the frequency.

The AC magnetic properties of ferrofluids, which are small (< 10 nm) magnetic particles dispersed in a liquid, show distinctly different behavior from that of bulk materials. There are two characteristic relaxation times, one due to Brownian relaxation caused by rotation of the particles in the liquid, and the other due to Néel relaxation caused by coherent rotation of the atomic spins within the particle [9, 10]. Both processes occur at frequencies well below the Larmor frequency f_0.

Nanocomposites have potential for two niche applications of soft magnetic materials. In low frequency applications, amorphous materials should continue to dominate, since they have the smallest hysteretic losses. Without significant eddy currents, only the small percentage of atoms required for glass forming do not contribute to the magnetization. However, at higher temperatures amorphous materials crystallize. In the current nanocrystalline materials [1-5], grain growth is limited by precipitation of additional phases, and a larger fraction of nonmagnetic atoms is needed. At higher frequencies, nanocomposites have potential advantages because they can have higher resistivity to reduce eddy current losses. While ferrites are currently used for high frequency applications because of their high resistivities, they have much lower magnetizations than iron-based alloys.

Iron-cobalt alloys are of interest for high temperature soft magnets because they have a high Curie temperature, high magnetization, and low coercivity. The value of the Curie temperature depends on the relative Co abundance. Iron-cobalt alloys have the largest magnetic moment per atom, and therefore large saturation magnetizations [11]. They have a low coercivity due to the low magnetocrystalline anisotropy K of the body-centered cubic structure. There is a zero crossing of the anisotropy near the equiatomic composition [12].

We investigate nanolaminates formed by compaction of FeCo nanoparticles with a very thin coating of a protective carbon or oxide. By choosing a particle or grain diameter well below the maximum monodomain size, the coercivity and hysteretic power losses can be minimized [1–3]. The coatings act as a barrier to eddy currents, reducing the eddy current power losses at high frequency. The goals are to minimize the portion of nonmagnetic atoms while retaining a stable nanocrystalline structure at high temperature, and to determine the degree of coating which retains significant exchange coupling for minimum K_{eff} while creating significant barriers to eddy currents.

2. EXPERIMENTAL

Particle Synthesis. Here the alloy nanoparticles were synthesized by the polyol method [13], a chemical route which leads to highly monodisperse metal particles. Iron chloride tetrahydrate and sodium hydroxide were dissolved in ethylene glycol and heated to 110 °C while stirring. A second solution of cobalt hydroxide in ethylene glycol at the same temperature was added, and the mixture was heated to 195 °C, where a precipitate formed. The total metal ion concentration was 0.2 M, and the hydroxide concentration was 2.0 M. Water and other reaction products were distilled off, and the solvent was refluxed for one hour at the maximum temperature. The precipitate was thoroughly washed with methanol, and dried.

While the particle size can be varied by changing the metal salt concentration and reaction time, the average grain diameter was roughly constant and approximately 20 nm. The composition was determined from electron energy loss spectroscopy [14]. The average grain size was obtained from Scherrer analysis of the x-ray diffraction peaks, and the particle size was found from transmission electron microscopy. The exchange length in magnetically soft materials like FeCo is large, and here is comparable to the grain size. Adjacent grains can then be exchange coupled to each other, leading to a further reduction in the anisotropy and coercivity, as explained by the random anisotropy model [1–3, 6].

Compaction. A nanocomposite has nanoparticle-sized grains, which may be dispersed in a matrix that mediates their coupling. The coupling strength depends on the magnetic behavior of the matrix and on the degree of coherence at the interface between the nanoparticles and the matrix. Exchange interactions may couple nanoparticles together. We worked with Dr. S. Sudarshan and Mr. Sang Yoo of Materials Modification, Inc., on plasma pressure compaction, which has the advantage of being able to reduce or remove the thin coating surrounding FeCo nanoparticles under ambient conditions. Powders were compacted by a combination of pressure and an electric arc in a two stage process. First a voltage pulse established a continuous current path across the sample in a graphite mold under a pressure of 10 MPa. This generated a plasma in the voids, and partly removed surface impurities such as oxides. In the second stage a continuous current path led to resistive sintering. The pressure was increased to 70 MPa to deform and compact the particles. The entire process required only a few minutes, thereby limiting grain growth. The resistive heating concentrated in the "necks" forming as the particles sinter, making them deform more

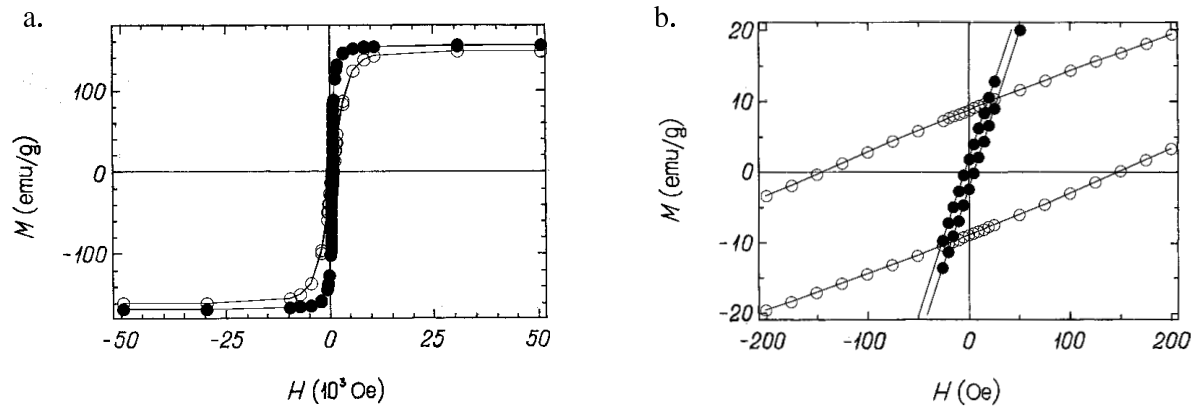

Fig. 1. a.) Comparison of $Fe_{10}Co_{90}$ nanoparticles made by the polyol method (open circles), and a compact made from them (filled circles); **b.)** An expanded region shows the coercivity of the pellet is on the order of 5 Oe, much less than that of the precursor particles, which is approximately 150 Oe.

readily. Compacts with over 90% theoretical density were made from the nanoparticle powders.

Magnetic Properties. There was a substantial amount of magnetic characterization, including SQUID magnetometry (with a Quantum Design MPMS) to determine the coercivity, and AC permeametry (with a Walker Scientific AC Hysteresisgraph) on toroidal compacts to measure the frequency dependence of the permeability m and the power loss. For the AC measurements, the toroid outer diameter was 2.54 cm, and it had a square cross section with dimensions 3.0×4.1 mm. There were 154 primary turns and 11 turns in the pickup coil. The amplitude of the AC magnetic field applied was 125 Oe, and the frequency ranged from 100 to 100,000 Hz. The temperature of the toroid was controlled by placing it in thermal contact with an ice bath (0°C), or with it inserted in a furnace (100 °C – 500 °C). At elevated temperatures the coils were sheathed with fiberglass sleeving (Omega Engineering, Inc.).

3. EXPERIMENTAL RESULTS

Fig. 1 shows a comparison of the DC hysteresis loops for the powder and compacted pellet of a typical sample. Compaction significantly reduces the coercivity, indicating that the exchange coupling is increased, as predicted by the random anisotropy model.

The AC hysteresis loops were measured for toroids cut from the same compressed pellets, for a range of frequencies. With AC excitation, the pickup loop measures the magnetic induction $B = 4\pi M + H$. Fig. 2 illustrates the characteristic behavior as a function of frequency. At low frequencies (Fig. 2a) the applied field H was sufficient to saturate the sample, reaching the single-valued region of $B(H)$. As the frequency was raised, the width of the hysteresis loop and therefore the coercivity increased, but the maximum induction remained approximately the same, up to a characteristic frequency (Fig. 2b). Approaching this frequency, the sample was no longer saturated at the maximum applied field, and the maximum magnetic induction dropped (Fig. 2c).

The permeability as a function of the maximum applied field is illustrated in Fig. 3, for several representative frequencies. Defining the permeability as the maximum value of B/H, it is expected to vary depending on the magnitude of H_{max}. If H_{max} is small and the sample is not saturated, B increases approximately linearly with H, and μ is large. If H_{max} is large and the sample is never saturated, B increases more slowly with increasing H and μ is reduced. In order to understand the fundamental physics of the AC excitation of the nanocomposites, a value of H_{max} = 125 Oe was selected for further measurements so that the samples were saturated at low frequency.

Several important quantities for soft magnetic materials were measured as a function of frequency. The real (in-phase) and imaginary (out-of-phase) parts of the permeability $\mu = B/H$ were also measured as a function of frequency (Fig. 4). In the low frequency range, the phase lag between B and H is small, and μ" is negligible. μ' is roughly constant up to the characteristic frequency, where it drops off sharply. μ" peaks as μ' drops off, and the critical frequency f_c is determined from the position of the peak in μ". The characteristic frequency of the permeability varied with temperature (Fig. 5). While the low frequency magnitude of m dropped off slightly with increasing temperature, due to a reduction in the magnetization, f_c rose substantially, from 1400 Hz at 0 °C to 6000 Hz at 500 °C. As noted in the hysteresis loops, the coercivity rose with increasing frequency (Fig. 6). It peaked at a frequency approximately 2-3 times f_c, and decreased somewhat at high frequencies. The overall power loss per cycle is shown in Fig. 7. At low frequencies it rises linearly, as expected from Eq. 2 if hysteretic losses are dominant.

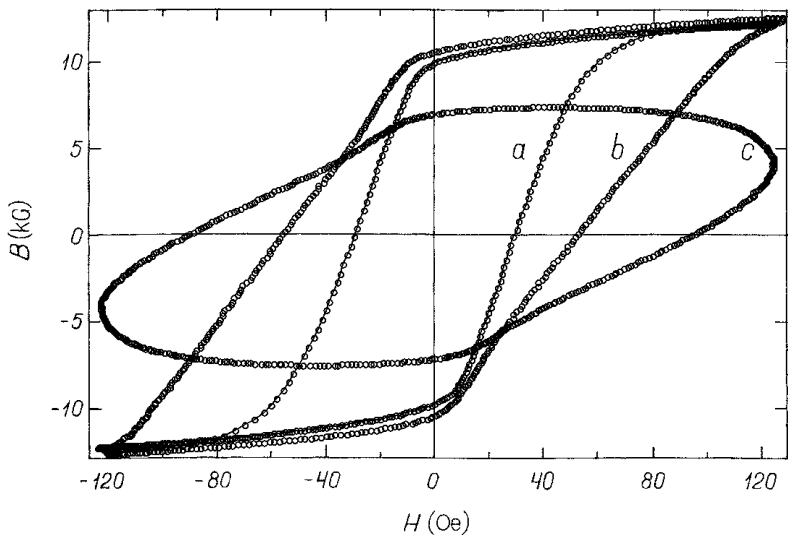

Fig. 2. AC Hysteresis loops for $Fe_{10}Co_{90}$, at 0 °C. **a.)** 100 Hz, **b.)** 800 Hz, **c.)** 5000 Hz.

At frequencies above f_c a weaker dependence is observed, closer to $f^{0.5}$. As the temperature is increased the power loss per cycle decreases somewhat, due mainly to the reduction in the coercivity.

4. MODEL OF AC MAGNETIC PROPERTIES

Our model of the AC properties of nanocomposites is based on a monodomain magnetic particle in an oscillating magnetic field. For a uniaxial particle with the applied field parallel to the easy axis, the energy E is given by

$$E = KV \sin^2\theta - M_s H \cos\theta, \qquad (3)$$

where K is the magnetocrystalline anisotropy, V is the particle volume, θ is the angle between the magnetization direction and the applied field H, and M_s is the saturation magnetization. Stoner-Wohlfarth theory [15-17] has shown that energy minima occur at θ = 0° or 180°, and a maximum exists where $\cos\theta = -HM_s/2K$.

In order to reverse the magnetization direction, the energy barrier must be overcome. If this does not occur within the measurement time, then hysteresis is observed. The rate of going over the barrier τ_0^{-1} is given by

$$\tau^{-1} = \tau_0^{-1} \exp\left(-\frac{\Delta E}{kT}\right), \qquad (4)$$

where $\tau_0^{-1} = f_0$ is the Larmor frequency, ΔE is the magnitude of the energy barrier, k is the Boltzmann constant, and T is the temperature.

If the magnetic field oscillates in time,

$$H(t) = H_0 \cos(2\pi f t), \qquad (5)$$

then the positions of the energy minima and maxima will also change with time, as shown in Fig. 8. Early in the cycle state 1 is the global minimum and state 2 is a local minimum, but later the roles are reversed. The height of the energy barrier which must be over-

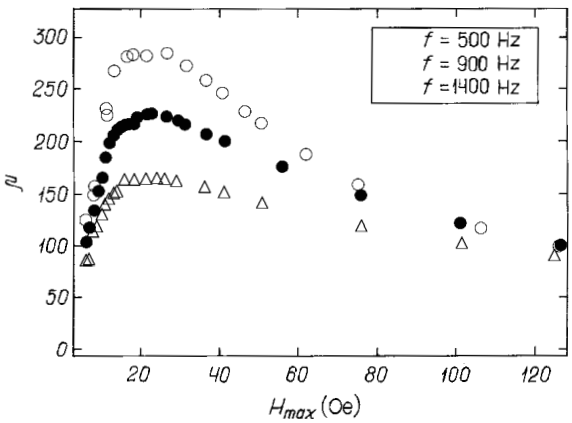

Fig. 3. Overall permeability for $Fe_{10}Co_{90}$, as a function of H_{max}, at 0 °C, for 500, 900, and 1400 Hz. The peak permeability at 22 Oe reflects where the slope of the *B(H)* starts to decrease.

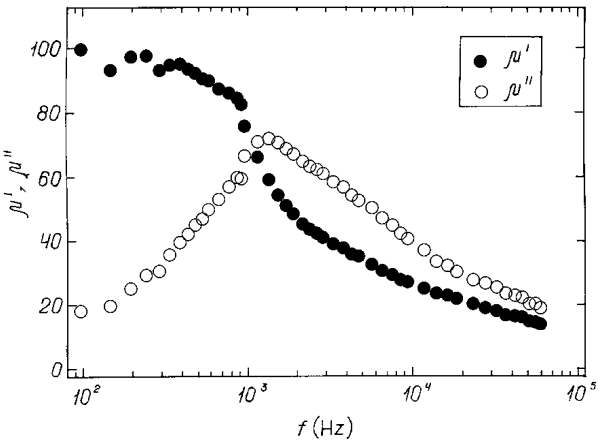

Fig. 4. The real (μ') and imaginary (μ") parts of the permeability for $Fe_{10}Co_{90}$, at 0 °C, as a function of frequency.

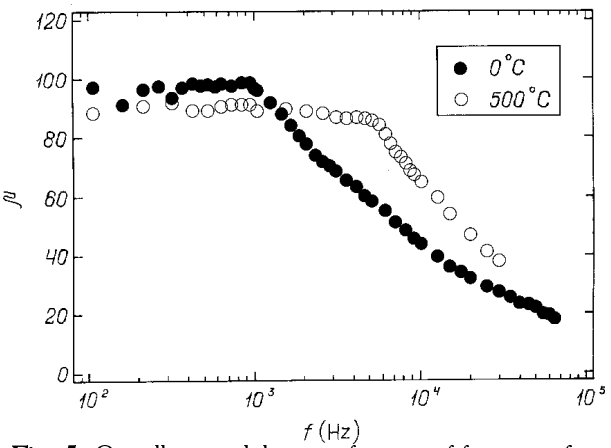

Fig. 5. Overall permeability as a function of frequency for $Fe_{10}Co_{90}$, at 0 °C and 500 °C.

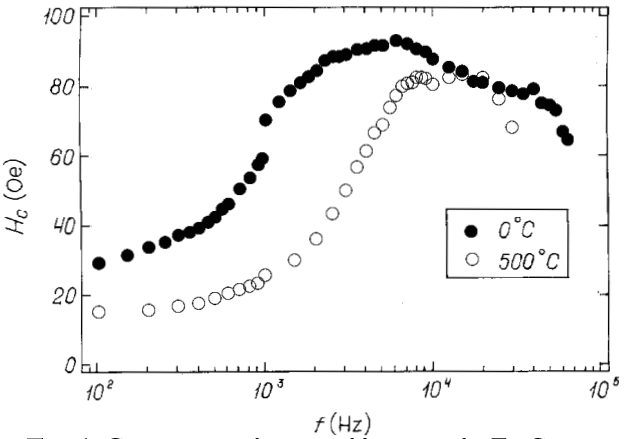

Fig. 6. Coercivity as a function of frequency for $Fe_{10}Co_{90}$, at 0 °C and 500 °C.

come for the particle to switch from the local to the global minimum also oscillates in time and is greatest at zero applied field.

Given an ensemble of particles and monitoring the population N_1 in state 1 and N_2 in state 2 as a function of time, the magnetization can be determined:

$$M(t) = M_S(N_1(t) - N_2(t)) = M_S(2N_1(t) - 1). \quad (6)$$

Here we assume that population is conserved, and that at all times

$$N_1 + N_2 = 1. \quad (7)$$

The population in state 1 as a function of time depends on the rate τ_{bkwd}^{-1} at which particles get over the barrier from state 2, and on the rate τ_{fwd}^{-1} that they leave state 1 in the forward direction over the barrier:

$$\frac{dN_1}{dt} = -\frac{dN_2}{dt} = \tau_{bkwd}^{-1} N_2 - \tau_{fwd}^{-1} N_1. \quad (8)$$

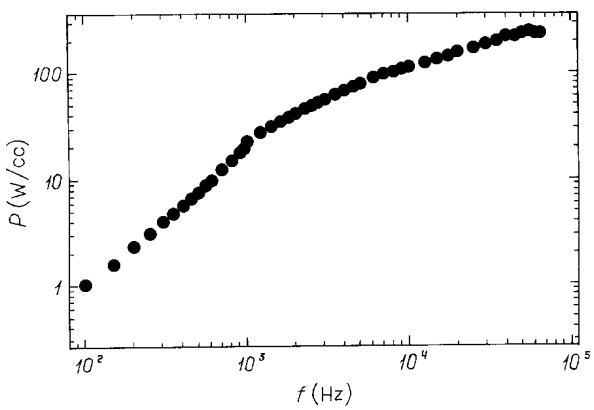

Fig. 7. Power Loss per unit volume as a function of frequency for $Fe_{10}Co_{90}$, at 0 °C.

Substituting for the rates using Eq. 4,

$$\frac{dN_1}{dt} = \tau_0^{-1}\left[(1-N_1)\exp\left(\frac{-\Delta E_{bkwd}}{kT}\right) - N_1\exp\left(\frac{-\Delta E_{fwkd}}{kT}\right)\right]. \quad (9)$$

Substituting for the forward ΔE_{fwd} and reverse ΔE_{bkwd} energy barriers,

$$\Delta E_{fwd} = E_{max} - E_1 = KV\left[1+\frac{HM_S}{2K}\right]^2 \quad (10a)$$

$$\Delta E_{bkwd} = E_{max} - E_1 = KV\left[1+\frac{HM_S}{2K}\right]^2 \quad (10b)$$

the differential equation becomes

$$\frac{dN_1}{dT} = \tau_0^{-1}\left[(1-N_1)\exp\left(\frac{-KV}{kT}\left[1+\frac{HM_S}{2K}\right]^2\right) - N_1\exp\left(\frac{-KV}{kT}\left[1+\frac{HM_S}{2K}\right]^2\right)\right]. \quad (11)$$

In an oscillating magnetic field $H(t)$, Eq. 11 must in general be solved numerically.

This problem has many similarities to that of an electric dipole in an AC electric field, which was originally solved by Peter Debye [18,19], with two main differences. In the electric dipole model, there was no equivalent to magnetocrystalline anisotropy, so the solution corresponds to the superparamagnetic limit. Also, in the electric dipole model, the factor equivalent to $x = M_S VH/kT$ is much less than one, and when e^x is approximated by $1+x$, the equation corresponding to Eq. 11 can be solved analytically.

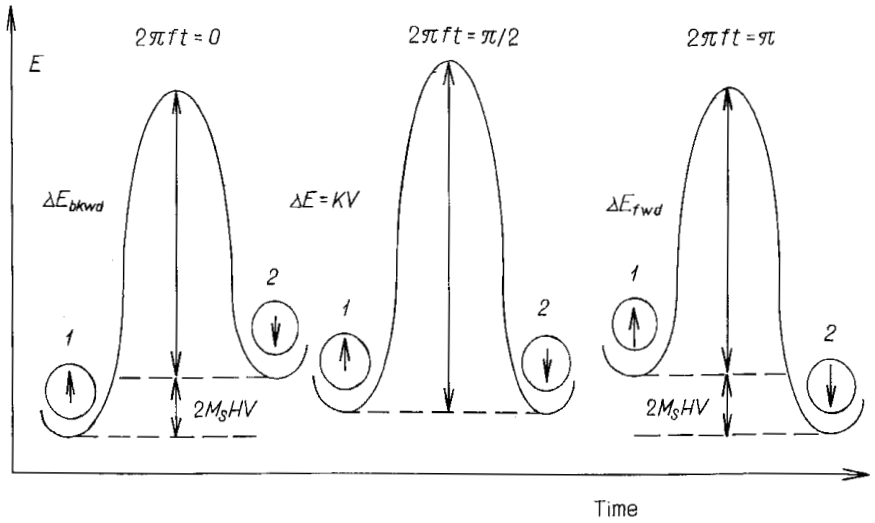

Fig. 8. Energy levels as a function of time, for different parts of the cycle of $H(t)$. Here E_1 is the energy of a particle in state 1, E_2 is the energy of a particle in state 2, and ΔE is the magnitude of the barrier between the local minimum and the maximum energy states.

Equation 11 can be solved analytically in the limit of large K, where $\Delta E_{fwd} \approx \Delta E_{bkwd}$. With the substitution

$$y = \frac{KV}{kT} \tag{12}$$

Eq. 11 then simplifies to

$$\frac{dN_1}{dt} \approx \tau_0^{-1} e^{-y}(1-2N_1). \tag{13}$$

The solution to Eq. 13 is given by

$$N_1(t) = \frac{1}{2}\left[1+\exp(-2\tau_0^{-1} yt)\right]. \tag{14}$$

There will be a characteristic or resonant frequency f_c, where

$$f_c = \frac{\tau_0^{-1} e^{-y}}{\pi} = \left(\frac{\tau_0^{-1}}{\pi}\right)\exp\left(\frac{-KV}{kT}\right), \tag{15}$$

where the population oscillates in resonance with the driving field $H(t)$. Above this frequency, the population shifts cannot keep up with the rapidly changing driving field.

The model breaks down for cases where $HM_S/2K > 1$, since this requires that $|\cos\theta = -HM_S/2K|$ be greater than one. To investigate the small K limit, which is of critical importance for soft magnetic materials, we reduced the amplitude of the magnetic field H_0 where necessary. In experiments it is possible to have large amplitudes of the AC magnetic field when studying materials with very low anisotropy. Here the sample is being driven past the high slope portion of the hysteresis curve during each half-cycle. In applications of soft magnetic materials, this is undesirable since the permeability $\mu = B/H$ is reduced. Therefore the model can be used to understand the AC magnetic behavior in situations of greatest technological importance.

5. MODELING RESULTS AND COMPARISON WITH EXPERIMENT

The simulation results show the same characteristics as the experimental data, and provide insight about the mechanism responsible for the frequency dependent behavior.

Fig. 9 illustrates the connection between the time-dependence of M and the $B(H)$ curves for driving fields of different frequencies $H=H_0\cos(2\pi ft)$. If the frequency is low enough (Fig. 9a) the sample has time to equilibrate with the slowly varying field and superparamagnetism is observed. There is a negligible phase lag θ between $M(t)$ and $H(t)$. Because of this $M(t)$ reaches its maximum value well below the maximum amplitude of the driving field H_0. At somewhat higher frequencies $M(t)$ starts to lag behind $H(t)$ significantly, leading to hysteresis (Fig. 9b). However $M(t)$ still reaches its maximum value before $H(t)$ starts to decrease. At the critical frequency f_c this is no longer true (Fig. 9c), and the shape of $M(t)$ and the hysteresis loop change noticeably. $B(H)$ no longer contains single valued regions, and the maximum value of B starts to decrease relative to its value at lower frequencies. At the highest frequencies $M(t)$ and $H(t)$ are almost completely out of phase and the maximum values of $M(t)$ and $B(H)$ are very small (Fig. 9d). The model simulates characteristics of the experimental results shown in Fig. 2, and shows that the shape and magnitude of

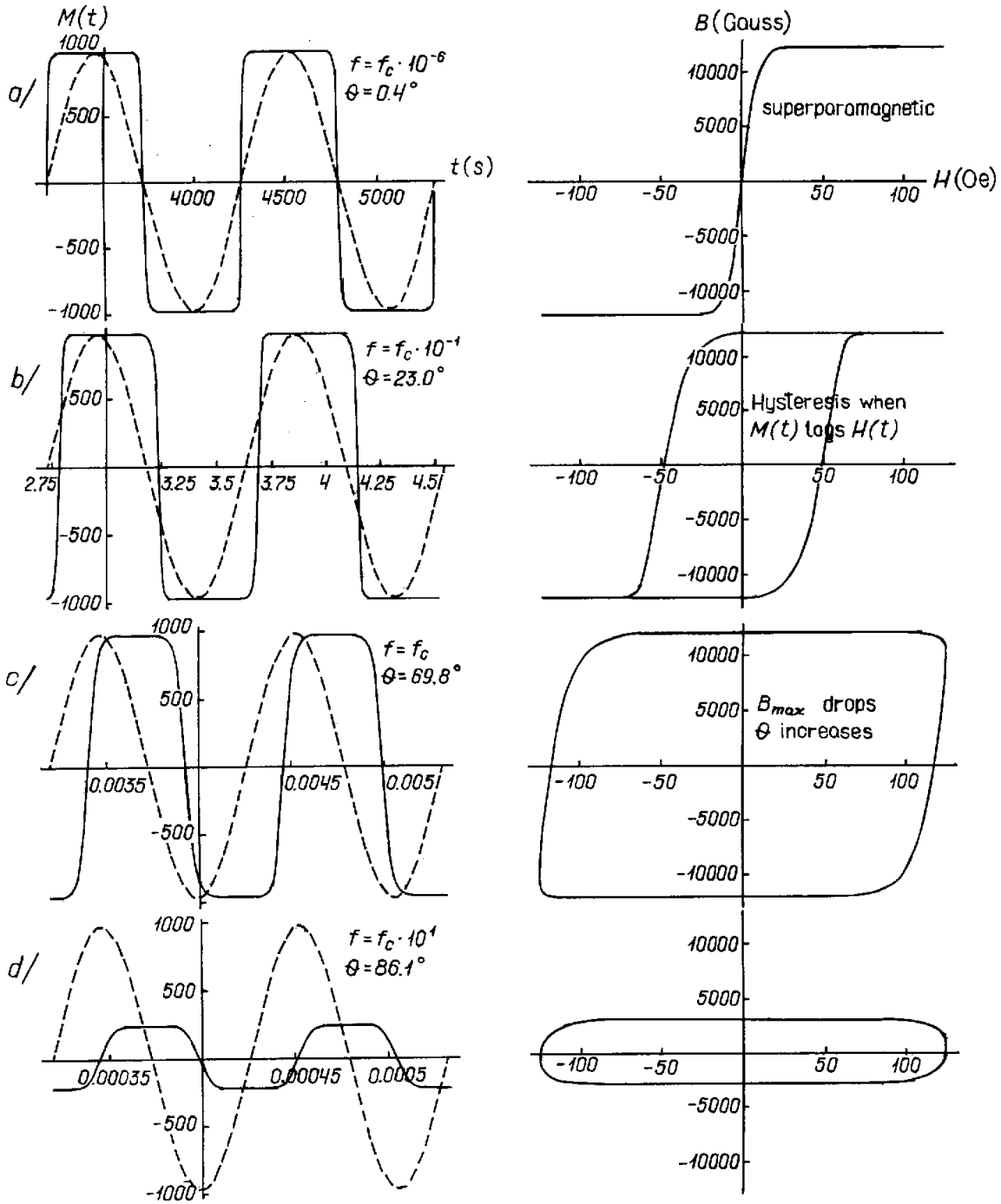

Fig. 9. *M(t)* and *H(t)*, and the corresponding *B(H)* curves for a sphere of exchange coupled volume *V* and effective anisotropy *K*. **a.)** for a superparamagnetic particle, **b.)** for a monodomain but not superparamagnetic particle at low frequency *f*, **c.)** at med. *f*, and **d.)** at high *f*. Note that in a.) and b.) *B(H)* appears to saturate, but this is because $4\pi M$ is so much larger than *H*. These simulations used the following parameters: M_S = 1000 emu/cc, H_0 = 125 Oe, *K* = $1.95 \cdot 10^5$ erg/cc, T=273 K, and *V* = $1.47 \cdot 10^{-18}$ cc. The critical frequency f_c was 1400 Hz.

B(H) depend on whether the magnetization of the exchange coupled volume within the sample can equilibrate with the changing external magnetic field.

Figure 10 shows the corresponding trend in the permeability μ as a function of frequency. At low frequencies it is constant and equal to the DC value, but as soon as *M(t)* is unable to reach its maximum value, B_{max} and therefore m begin to drop, approaching zero in the high frequency limit. This is in contrast to the experimental results shown in Fig. 5, where μ decays more slowly. Such a difference would arise if the sample contained a distribution of characteristic frequencies f_c, perhaps related to a distribution of grain sizes.

Fig. 11 reveals the behavior of the simulated coercivity as a function of frequency. At low frequencies it follows Sharrock's Law [20]:

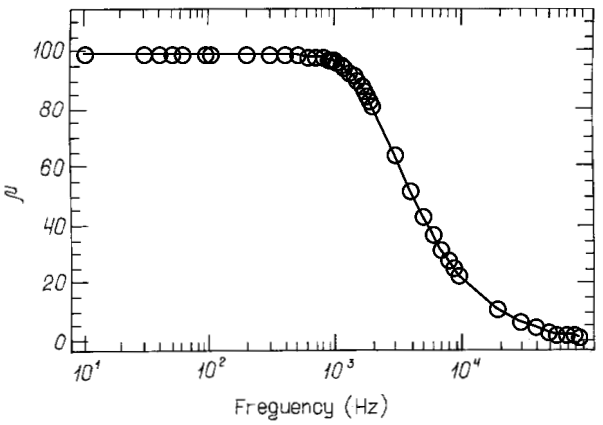

Fig. 10. The permeability $\mu = B_{max}/H_{max}$ as a function of frequency, for the same parameters as in Fig. 9.

$$H_c(f) = \left(\frac{2K}{M_S}\right)\left[1-\left(\frac{kT\ln(f_0/f)}{KV}\right)^{1/2}\right], \qquad (16a)$$

or

$$H_c(f) = \left(\frac{2K}{M_S}\right)\left[1-\left(\frac{kT}{KV}\right)^{1/2}\left(\frac{1}{2}\right)\ln f_0\right] + \left(\frac{2K}{M_S}\right)\left[\left(\frac{kT}{KV}\right)^{1/2}\right]\left(\frac{1}{2}\right)\ln f_0 \qquad (16b)$$

rising with the log of the frequency. The peak in H_c occurs between two and three times f_c, and then H_c begins to decrease. This occurs when the magnetization due to the driving field is low enough, and the value of $H(t)$ needed to make $M(t)$ equal to zero is reduced. The experimental coercivity shown in Fig. 6 also rises and peaks at roughly the same frequency, but the rise is not proportional to $\ln f$. While there may be a region where H_c obeys this functional dependence, there appears to be a low frequency contribution to the coercivity from a factor not included in the model. This could arise from particles not exchange coupled to their neighbors, possibly from a thicker coating.

Fig. 12 shows the hysteretic power loss P_{hys} found from the are of the hysteresis loop $B(H)$, as a function of frequency. This rises linearly at low frequencies, as expected from Eq. 2, but then it levels off at f_c. At very high frequency it should decrease when both M_{max} and H_c are decreasing.

In comparison, Fig. 7 shows the total experimental power loss. At frequencies below f_c, hysteretic power losses dominate. This is expected for frequencies below 10,000 Hz.

The qualitative behavior illustrated in Fig. 9-12 is similar for a wide range of input parameters; only the magnitudes of μ, H_c and P_{hys} vary, along with the critical

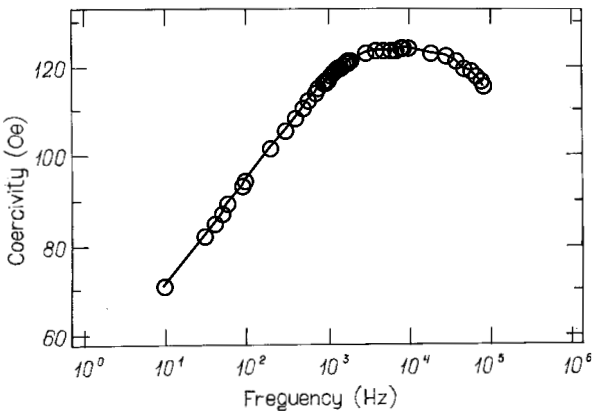

Fig. 11. The coercivity H_c as a function of frequency, for the same parameters as in Fig. 9.

frequency f_c. The dependence of f_c on the anisotropy, volume, and temperature is summarized in Fig. 13. From the simulated data, an empirical functional form for $f_c(K,V,T)$ was obtained:

$$f_c = 10^{-9}\tau_0^{-1}\exp\left[-(5.88\cdot10^{15}K/erg)\left(\frac{KV}{T}\right) - (4.33\cdot10^{-6}cc/erg)K + (4.11\cdot10^{20}K/cc)\left(\frac{V}{T}\right) + 18.98\right]. \qquad (17)$$

Note that this formula is considerably more complex than Eq. 15, which was valid only in the limit of large K. For soft magnetic materials K is small, and numerical simulations are the only was to predict the cutoff frequency.

For the experimental grain size, r =10 nm, and an effective anisotropy equal to $1.5\cdot10^5$ erg/cc would be needed to fit the observed room temperature value of f_c. The is a much larger value of the anisotropy estimated from the experimental coercivity and Sharrock's Law. Presumably the physically relevant volume V is not that of a single grain, but of a small number of coupled grains.

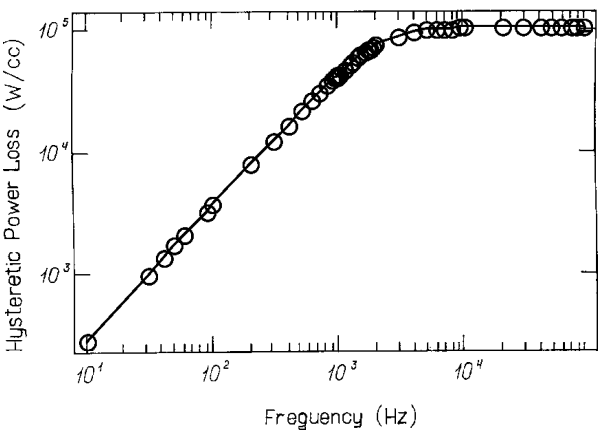

Fig. 12. The hysteretic power loss as a function of frequency, for the same parameters as in Fig. 9.

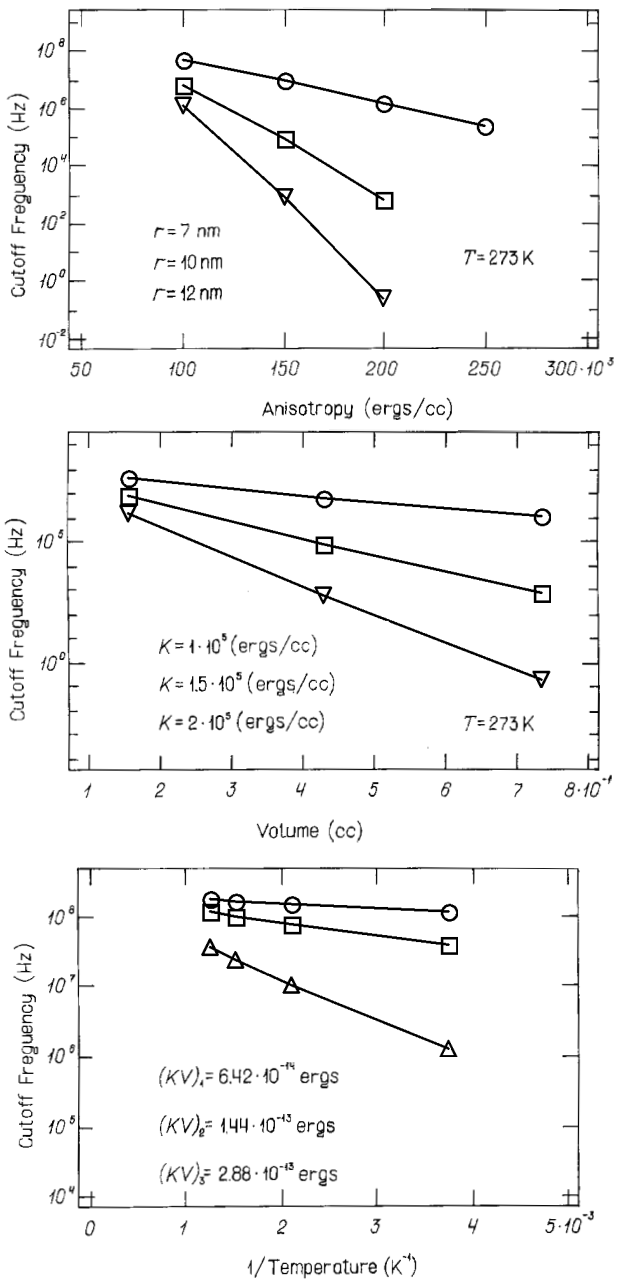

Fig. 13 a.) f_c as a function of the anisotropy for spheres of different radii. Here $V=(4\pi/3)r^3$; **b.)** f_c as a function of the volume; **c.)** f_c as a function of the inverse temperature.

6. CONCLUSIONS

The AC magnetic properties of soft magnetic nanocomposites made from compaction of $Fe_{10}Co_{90}$ nanoparticles can be understood in terms of an effective anisotropy and a related exchange coupled volume. The permeability is constant and equal to the DC value for low frequencies, but drops off above a characteristic frequency f_c. For bulk materials such as ferrites the cutoff frequency can be extremely high, and the behavior is understood in terms of the Landau-Lifshitz-Gilbert equation [21-23]. However for compacted nanocomposites the cutoff frequency is much lower, and depends on the sample microstructure. The value of this frequency can be increased by raising the temperature, or by reducing the anisotropy and grain size. Experiments are in progress to prepare samples to further test this model.

ACKNOWLEDGMENTS

This work was supported in part by the National Science Foundation under Grant numbers DMR-9900550 and ECD-8907068, and by the Air Force Office of Scientific Research under grant number F49620-96-1-0454. The assistance of K. Humfeld and N. Ide in the simulations is greatly appreciated.

REFERENCES

[1] G. Herzer // *IEEE Trans. Mag.* **25** (1989) 3327.
[2] G. Herzer // *IEEE Trans. Mag.* **26** (1990) 1397.
[3] G. Herzer // *J. Magn. Magn. Mater.* **112** (1992) 258.
[4] Y. Yoshizawa, S. Oguma and K. Yamauchi // *J. Appl. Phys.* **64** (1988) 6044.
[5] A. Makino, T. Hatani, Y. Naitoh, T. Bitoh, A. Inoue and T. Masumoto // *IEEE Trans. Mag.* **33** (1997) 3793.
[6] R. Alben, J. J. Becker and M. C. Chi // *J. Appl. Phys.* **49** (1978) 1653.
[7] N. Ashcroft and D. Mermin, *Solid State Physics* (Harcourt Brace, NY, 1976).
[8] R. A. McCurrie, *Ferromagnetic Materials: Structure and Properties* (Academic Press, NY, 1994).
[9] J. Zhang, C. Boyd and W. Luo // *Phys. Rev. Lett.* **77** (1996) 390.
[10] M. I. Shliomis and V. I. Stepanov, in *Advances in Chemical Physics*, ed. W. Coffey (Wiley, NY, 1987) **87** 1.
[11] C. W. Chen, *Magnetism and Metallurgy of Soft Magnetic Materials* (Dover, NY, 1986).
[12] F. Pfeifer and C. Radeloff // *J. Magn. Magn. Mat.* **19** (1980) 190.
[13] G.Viau, F. Fievet-Vincent and F. Fievet // *J. Mater. Chem.* **6** (1996) 1047.
[14] J. H. J. Scott, Z. Turgut, K. Chowdary, M. E. McHenry and S. A. Majetich // *Mat. Res. Soc. Symp. Proc.* **501** (1998) 121.
[15] E. C. Stoner and E. P. Wohlfarth // *Phil. Trans. Roy. Soc.* **A240** (1948) 599.
[16] W. F. Brown, Jr. // *J. Appl. Phys.* **29** (1958) 470.
[17] W. F. Brown, Jr. // *J. Appl. Phys.* **30** (1959) 130.
[18] A. K. Jonscher, *Dielectric Relaxation in Solids* (Chelsea Dielectrics Press, Ltd., London, 1983).
[19] P. Debye, *Polar Molecules* (Chemical Catalog Co., NY, 1929).

[20] M. P. Sharrock // *IEEE Trans. Mag*. **26** (1990) 193.
[21] L. Landau and E. Lifshitz // *Phys. Z. Sowjetunion* **8** (1936) 153.
[22] T. L. Gilbert, *Ph. D. thesis*, Illinois Institute of Technology, Chicago, IL, June 1956.
[23] H. B. Callen // *J. Phys. Chem. Solids* **4** (1958) 256.